ELSEVIER

Earth and Planetary Science Letters 202 (2002) 303–320

EPSL

www.elsevier.com/locate/epsl

Convective destabilization of a thickened continental lithosphere

C. Morency [a,*], M.-P. Doin [a], C. Dumoulin [b]

[a] *Ecole Normale Superieure, Laboratoire de Geologie, 24 rue Lhomond, 75231 Paris Cedex 05, France*
[b] *Université Joseph Fourier, Maison des Geosciences, LGIT, P.O. Box 53, 38041 Grenoble Cedex 9, France*

Received 20 November 2001; received in revised form 13 May 2002; accepted 3 June 2002

Abstract

Removal or delamination of the lithospheric mantle in a late stage of mountain building is a process often invoked to explain syn orogenic extension, high temperature metamorphism, magmatism and uplift. One mechanism that could explain the lithospheric root detachment is the development of convective instabilities within the peridotitic lithosphere due to its high density. This mechanism is studied by two-dimensional convective numerical simulations in the simple case of a strongly temperature dependent viscous rheology appropriate for upper mantle rocks. We neglect here the weakening effect of a brittle rheology and of a crustal layer, and therefore we did not model tectonic deformations. Depending on the upper mantle viscosity and activation energy, a 300 km thick root can be inferred to be either indefinitely stable or to thicken with time or to thin with time. When the lithosphere is initially thicker than its equilibrium thickness, the convective flow at the base and on the sides of the lithospheric root is strong enough to cancel downwards heat conduction and to progressively remove the root. This flow is due to the finite density perturbations induced by the topography of the isotherms on the base and at the sides of the root. We derive two general parameterizations of the convective removal duration as a function of the equilibrium thickness, the thickening factor, the root width, and the rheological temperature scale. Using these relationships, and assuming that the lithospheric equilibrium thickness is about 100 km, the removal duration of a 250 km thick root ranges from 55 to 750 Myr depending on the root width. It is too small to explain the long term stability of cratonic lithospheric root, but too long to explain any sudden change in the stress and strain states in mountain belts development.

Keywords: delamination; convection; time scales

1. Introduction

A possible consequence of orogenic building by thrusting or homogeneous thickening is to lead to a thickened lithosphere, whose isotherms are then stretched downwards. Such a root, colder and denser than the surrounding mantle, can be unstable, detach and sink into the mantle [1]. This fast or slow event strongly modifies the *P–T–t*

* Corresponding author. Tel.: +33-1-44-32-22-03; Fax: +33-1-44-32-22-00.
E-mail addresses: morency@geologie.ens.fr (C. Morency), doin@geologie.ens.fr (M.-P. Doin), caroline.dumoulin@obs.ujf-grenoble.fr (C. Dumoulin).

0012-821X/02/$ – see front matter
PII: S0012-821X(02)00753-7

paths recorded by crustal rocks and the states of stress and strain in the belt [2]. Removal of the lithospheric root is then often proposed to explain uplift, high temperature metamorphism, and the development of syn orogenic extension in an orogenic belt. England and Houseman [3] and England [4], studying the Tibetan Plateau, argued that the highly potassic volcanism there results from rapid heating of the mechanical boundary layer (m.b.l.), a consequence of removal of the lower lithosphere and its replacement by hot asthenosphere. The same scenario of mantle thinning was advanced for the Appalachian orogenesis on the basis of the reflective properties of the lower crust [5]. What mechanism could allow the removal of the mantle lithosphere and which time scale would be involved?

Three classes of possible physical mechanisms have been proposed. All are based on the excess weight of the root with respect to the asthenospheric mantle. Bird and Baumgardner [6] proposed a delamination process, during which the whole mantle lithosphere peels away at the favor of an intracrustal decoupling level and sinks into the asthenosphere leading to strong crust warming. Such a mechanism may lead to a short removal duration of about 10 Myr and to a rapid isostatic uplift. Rapid root breakoff could also be the consequence of highly non-linear rheology in high stress and strain regime involving whole-scale tectonic deformation ([7], e.g. extremely weak brittle rheology). The third mechanism is based on the development of convective instabilities within the mantle ductile part of the lithosphere [8]. In this paper, we focus on the latter mechanism.

Houseman et al. [8] consider an isoviscous fluid beneath a rigid layer. Such a model allows a thick part of the lithosphere to be removed in a few tens of Myr. In studies with a temperature and pressure dependent viscosity, the rigid upper layer is a high viscosity layer that is self consistently defined by its temperature structure [9–12]. In these cases only a thin layer with a low viscosity between the rigid and purely conductive mantle lithosphere and the asthenosphere can be quickly removed. However, despite this fundamental result, the estimated removal durations vary between 10 Myr [13,14] and a few hundreds of Myr [9]. Some numerical results also show that a thick lithospheric root could remain indefinitely stable [15]. Clearly these differences should come from the use of different upper mantle viscosities and from different temperature dependence of the viscosity. The question also arises on whether the destabilization duration will depend on the geometry of the thickened root: will a mantle lithosphere thickened by subduction along a few successive suture zones [16] be removed quicker than a homogeneously thickened root over a wide area?

We propose to parameterize the duration of convective removal of a homogeneous and instantaneously thickened lithosphere, and to identify precisely the thinning mechanism. In a first step, we define the model setup and the equilibrium state, towards which the thickened lithosphere will finally tend. We describe the mantle flow generated by the presence of the lithospheric root and its destabilization. In a second and third part we derive two relationships parameterizing the convective removal durations, depending on the geometry of the thickened root. These relationships are then used to propose and discuss scaled durations for root destabilization.

2. Simulations of the lithospheric root thinning in a convecting mantle

2.1. Model setup

We use a two-dimensional (2-D) numerical code [17] that solves in the Boussinesq approximation the conservation equations for mass, momentum (with infinite Prandtl number), and energy:

$$\vec{\nabla}\cdot\vec{u} = 0 \tag{1}$$

$$\vec{\nabla}\cdot\vec{\sigma} + \rho_{\mathrm{ref}}(1-\alpha(T-T_{\mathrm{ref}}))\vec{g} = 0 \tag{2}$$

$$\rho_{\mathrm{ref}} C_p(\partial T/\partial t + \vec{u}\cdot\vec{\nabla}T) - k\nabla^2 T - q = 0 \tag{3}$$

where $\vec{u}$ and $\vec{\sigma}$ are the velocity vector and total

Table 1
Normalization

Variables names	Symbols	Box normalization
Depth	z	$z^* = z/H$
Age	t	$t^* = \kappa t/H^2$
Temperature	T	$T^* = T/\Delta T$
Heat transfer by localized convection	Φ	$\Phi^* = \Phi H/k\Delta T$
Effective temperature drop	ΔT_{eff}	$\Delta T^*_{eff} = \Delta T_{eff}/\Delta T$
Cut-off temperature	T_q	$T^*_q = T^*_i - \Delta T^*_{eff}$
Thermal equilibrium thickness	z_{eq}	$z^*_{eq} = z_{eq}/H$
Activation energy	E	$E^* = E/nR\Delta T$
Activation volume	V	$V^* = V\rho gH/nR\Delta T$

R is the universal gas constant, g the gravity acceleration.

stress tensor, respectively, and other symbols are described in Tables 1–3. Adiabatic and shear heating in the energy Eq. 3 are neglected, except for two cases computed in the extended Boussinesq approximation (EBA). We consider a cartesian box of aspect ratio 3 (or 4) with a 151×51 (or 201×51), irregular grid mesh, refined in the upper third of the box and at the box base. The box is either heated from within (and the bottom of the box is assumed to be adiabatic) or from below (and the bottom of the box is isothermal). Non-dimensional variables are denoted by a * exponent and are described in Table 1. Non-dimensional temperature at the top of the box is fixed to 0. For comparison with the Earth's mantle, non-dimensional variables will be scaled in Section 5.3 using the parameters of Table 2.

The rheology is Newtonian ($n=1$) except for a few cases computed with a non-Newtonian rheology ($n=3$). The viscosity either depends exponentially on temperature T and depth z (Eq. 4) or follows an Arrhenius law (Eq. 5):

$$v^* = A^* \dot{\varepsilon}^{*-1+1/n} \exp\left(-\frac{b}{n}T^* + \frac{c}{n}z^*\right) \quad (4)$$

$$v^* = B^* \dot{\varepsilon}^{*-1+1/n} \exp\left(\frac{E^* + z^*V^*}{T^*_0 + T^*}\right) \quad (5)$$

where $\dot{\varepsilon}^*$ is the second invariant of the strain rate tensor and $T^*_0+T^*$ is the absolute temperature. This rheology is suited to study the flow at the base of the lithosphere and in the mantle. The high temperature dependence of viscosity leads to the formation of a rigid and conductive upper thermal boundary layer (u.t.b.l.) [18]. The temperature and viscosity drops across this stagnant lid are large, and the temperature within the convective cells, T^*_i, is rather homogeneous. In the lid, the temperature structure obeys the conduction equation. In this paper, we neglect the influence of surface and whole-scale lithospheric deformation on delamination. Modeling this process would require at least to introduce a realistic brittle–ductile rheology with a viscosity strongly depending on temperature and composition (crust/mantle) that limits the strength of the lithosphere at low temperature. We therefore impose a rigid top boundary condition, that further ensures that no deformation occurs in the upper part of the lithosphere. We set a free slip closed boundary condition at the base and on the sides of the box.

2.2. Initial thermal state and localized convection

Studying the convective removal of a thickened lithospheric root requires that we know, at least

Table 2
Variable names and values used for mantle scaling

Parameters	Symbols	Values
Internal mantle temperature	T_i	1300°C
Thermal equilibrium thickness	z_{eq}	100 km
Thermal expansion coefficient	α	3×10^{-5} K^{-1}
Thermal diffusivity	κ	10^{-6} m^2/s
Thermal conductivity	k	3.1 W/m/K
Heat capacity	C_p	1.25 kJ/kg/K
Density	ρ_{ref}	3300 kg/m^3
Activation energy (dry/wet)	E	300/240 kJ/mol
Activation volume (dry/wet)	V	6/5 cm^3/mol

as a reference, towards which stable state (or equilibrium thickness) the lithosphere will ultimately evolve. Therefore, we first perform convection simulations until they reach a statistically steady state, defined when the short time scale averages of surface heat flow, bottom heat flow, internal temperature, and velocities remain constant with time.

We performed simulations at large Rayleigh numbers, for which one obtains a relatively flat rigid lid and a turbulent localized convection in the form of small-scale instabilities dripping from the base of the rigid lid [19]. The flow in the unstable sublayer at the base of the lithosphere follows the isotherms slope and carries cold material towards topographical tips from which blobs originate. This regime is favored by internal heating, non-Newtonian rheology, and large aspect ratio boxes. It should control the equilibrium thickness of a fertile continental lithosphere when there is plate tectonics [19,20]. We here summarize parameterization obtained for the heat flow Φ_{eq} transferred by localized convection at equilibrium.

A small effective temperature drop in the unstable layer below the lid, ΔT^*_{eff}, drives localized convection. It scales proportionally to the rheological temperature scale δT^*_ν, with:

$$\delta T^*_\nu = -\left(\frac{\partial \ln \nu^*}{\partial T^*}\right)^{-1} \tag{6}$$

this derivative being calculated across the base of the lid [21–25]. δT^*_ν corresponds to the temperature change for an e-fold viscosity contrast. In case of an exponential rheology (Eq. 4), it yields:

$$\delta T^*_\nu = \left(\frac{2}{n+1}(b-\alpha_n c/\Phi^*_{eq})\right)^{-1} \quad [19,26] \tag{7}$$

where α_n is a corrective term in pressure equal to 1 when $n=1$ and to 2.6 when $n=3$. In case of an Arrhenius rheology (Eq. 5), δT^*_ν writes as:

$$\delta T^*_\nu = \left(\frac{2}{n+1}\left(\frac{nE^*}{(T^*_0+T^*_i)^2}+\frac{nV^*(T^*_i-\alpha_n(T^*_0+T^*_i))}{(T^*_0+T^*_i)^2\Phi^*_{eq}}\right)\right)^{-1} \tag{8}$$

The equilibrium thickness of the u.t.b.l., z^*_{eq}, is defined as the depth at which the conductive geotherm crosses $T^* = T^*_i$.

Convective motion at the base of the lithosphere can be parameterized using a Rayleigh number, Ra_{BL}, defined as:

$$Ra_{BL} = \frac{\alpha\rho g\Delta T H^3}{\kappa \nu_{BL}} \tag{9}$$

where ν_{BL} is the viscosity in the asthenosphere. In the turbulent regime, one may assume that the u.t.b.l. is in a marginal stability state, i.e. that a cold drip develops when the local Rayleigh number of the u.t.b.l. exceeds a critical value Ra_c [27–29]. For a fluid with a temperature dependent viscosity and for rigid-free boundary conditions, Ra_c equals $21(T^*_i/\delta T^*_\nu)^4$ [21], where $\delta T^*_\nu/T^*_i$ represents the rheological temperature scale in the reference frame of the u.t.b.l. The boundary layer stability analysis yields:

$$\Phi^*_{eq} = \left(\frac{Ra_{BL}}{Ra_c}\right)^{1/3} T^{*4/3}_i \tag{10}$$

This expression yields a scaled heat flow at the lithospheric base independent of the box (mantle) thickness, but depending only on local parame-

Table 3
Parameters

Parameters	Symbols
Stress exponent	n
Box temperature drop	ΔT
Box height	H
Radiogenic heat production	q
Rheological temperature scale	δT_ν
Internal temperature	T_i
Viscosity	ν
Lithospheric root width	x
Stretching factor	γ
Root removal duration	t_{2-D}
Removal duration predicted by 1-D conductive model	t_{1-D}

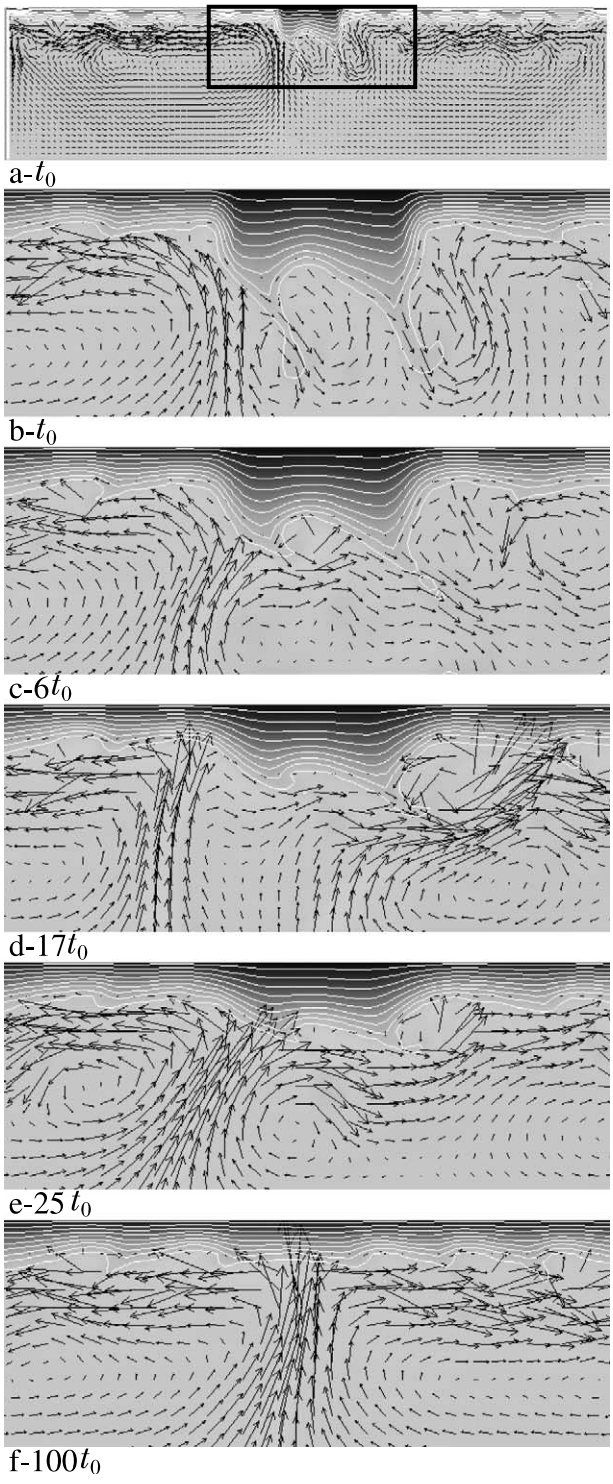

Fig. 1. Zoom, located by the black rectangle on panel (a), on the temperature evolution of the root, after thickening by a factor 2.5, displayed at different time steps ($t^*_0 = 10^{-4}$, scaled to $t_0 \approx 4$ Myr) on panels (b) to (f). The width and thickness of display zoom boxes are 1.28 and 0.50, respectively. This simulation corresponds to case 21 in Table 5, with $x^* = 0.40$.

ters. It is consistent with the relationship:

$$\Phi^*_{eq} \approx 0.5(Ra_{BL}\delta T^{*4}_v)^{1/3} \quad (11)$$

that has been obtained by numerical simulations and experiments for non-Newtonian and Newtonian rheologies and for fluids heated from within or from below or cooled from above [19,25,26,30,31]. This indicates that hot upwellings originating from the lower thermal boundary layer only influence Φ_{eq} through increasing the interior temperature T_i, and thus reducing the viscosity below the u.t.b.l., ν_{BL}.

2.3. Description of the flow during root destabilization

Using the temperature field resulting from turbulent simulations, we then simulate the instantaneous formation of a thickened lithospheric root by stretching downwards the isotherms. We apply a constant thickening factor γ either to the entire u.t.b.l. or across a limited width x^* (see for example Fig. 1a). The initial thickness of the thickened lithospheric root thus becomes γz^*_{eq}. We then simulate the thermal evolution of the lithospheric root when it returns towards equilibrium (z^*_{eq}) (Fig. 1), using different values for x^*, γ, Ra_{BL} and rheologies. All simulations discussed and displayed in this paper are listed in Tables 4 and 5.

A zoom on the lithospheric root evolution through time is shown on Fig. 1b–f. We note that there is an unstable layer at the base of the u.t.b.l. and on the sides of the thick root. In the case of Fig. 1, the strong temperature dependence in the Arrhenius rheology yields a small temperature drop across the unstable layer, ΔT^*_{eff}, of about 0.09. We can see that the area in the lithosphere with a temperature lower than about $T^*_i - \Delta T^*_{eff}$ is rigid. This is also the case in all simulations with a low thickening factor or with a strongly temperature dependent viscosity. When the thickening factor is large and for an exponential rheology with $b \leq 13$, the high stresses due to the strong initial heterogeneities in density induce strain within the lithospheric root, and therefore a whole-scale deformation of the thickened lithosphere. Small-scale drips then merge into large

Table 4
Simulation table for a fluid with a viscosity depending exponentially on temperature and depth

n^0	b	c	Ra_{BL}	Φ^*_{eq}	ν^*_{BL}	z^*_{eq}	T^*_i	γ	x^*
1	18	0	2.21×10^8	6.1	$10^{-7.39}$	0.16	0.945	2.5	w.b.l.
2	18	0	4.38×10^8	8.5	$10^{-7.34}$	0.11	0.939	2.5	w.b.l.
3	16	0	3.93×10^8	9.3	$10^{-6.45}$	0.10	0.928	1.5	w.b.l.
4	16	0	3.93×10^8	9.3	$10^{-6.45}$	0.10	0.928	2.5	**0.80**, **0.40**, **0.20**
5	16	0	6.63×10^8	11.6	$10^{-6.44}$	0.08	0.927	1.5	w.b.l.
6	13	4.2	2.36×10^7	5.7	$10^{-4.18}$	0.14	0.786	1.5	w.b.l.
7	13	4.2	2.36×10^7	5.7	$10^{-4.18}$	0.14	0.786	2	w.b.l., 1.00
8	13	4.2	2.36×10^7	5.7	$10^{-4.18}$	0.14	0.786	2.5	w.b.l., 2.75, 2.55, 2.16, 1.57, **1.00**, **0.80**, **0.60**, **0.40**, **0.20**, **0.12**
9	13	4.2	2.36×10^7	5.7	$10^{-4.18}$	0.14	0.786	3	w.b.l., 1.00
10	13	4.2	2.36×10^7	5.7	$10^{-4.18}$	0.14	0.786	3.5	1.00
11	13	4.2	4.48×10^8	11.4	$10^{-4.37}$	0.07	0.797	1.5	w.b.l.
12	13	4.2	1.30×10^8	9.4	$10^{-4.12}$	0.08	0.755	1.5	w.b.l.
13	13	4.2	3.95×10^7	6.5	$10^{-4.20}$	0.12	0.783	1.5	w.b.l.
14	13	0	3.04×10^8	11.4	$10^{-5.16}$	0.08	0.914	1.5	w.b.l.
15	13	0	3.04×10^8	11.4	$10^{-5.16}$	0.08	0.914	2	**0.40**
16	13	0	3.04×10^8	11.4	$10^{-5.16}$	0.08	0.914	2.5	**0.20**
17	13	0	2.17×10^8	10.1	$10^{-5.13}$	0.09	0.909	1.5	w.b.l.
18	11.08	4.2	2.21×10^7	5.6	$10^{-3.52}$	0.14	0.784	1.5	w.b.l.
19	11.08	0	6.85×10^7	8.2	$10^{-4.33}$	0.11	0.900	1.5	w.b.l.

In all these simulations the box is heated from below, the aspect ratio is 3. 'w.b.l.' points to simulations where the lithosphere has been thickened over the whole box length. Bold numbers mark simulations where the main destabilization mechanism is due to flow on the root sides.

cold downwelling structures that are stretched until the bottom of the box (Fig. 2). The modeled whole-scale lithospheric deformation there derives from employing a viscosity in the lithospheric mantle that depends too moderately on temperature.

The convective removal of the lithospheric root can be viewed as resulting from two mechanisms (see Fig. 3): (1) heating and thinning of the rigid part of the lithosphere occurs because the heat transferred through it by conduction is initially lower than that brought by sublithospheric localized convection (Φ^*). (2) Convection on the edges of the root tends to erode it by the sides, thus reducing its width x^*. In the following we quantify the mean thinning and shortening rates of the root for each simulation.

Note that the thickening procedure in our simulations increases the initial slope of the isotherms at the base of the thickened root. Furthermore, the flow in the unstable sublayer always follows the topography of isotherms and brings cold material towards the topographical tips. This, in the first few simulation steps, enhances isotherm topography, which will later decay. The root thus presents strong lateral heterogeneities that introduce large uncertainties in the determination of the mean thinning and shortening rates. However, if we had set initially a simple step-like structure for the transition between the equilibrium state and the root (with flat isotherms within each portion), the flow would have, in a first stage, only developed on the root sides. The onset of flow at the base of the u.t.b.l. along its flat portions would have been delayed by a few tens of Myr (20–50 Myr, scaled using values displayed in Table 2), corresponding to the growth time of initially infinitesimal perturbations [32]. This is for example what happens in King and Ritsema [33]. We argue that, whatever the initial thickening mechanism is, it will not produce flat isotherms within each lithospheric portion. Therefore, due to these finite thermal perturbations at the base of the root, convective motions leading to root removal are fully developed even at the start of the simulation (Fig. 1a).

2.4. Estimation of the destabilization duration

To estimate the destabilization duration, t^*_{2-D}, we follow the temperature evolution at a fixed depth close to the equilibrium depth ($z^* = 0.9z^*_{eq}$) and averaged over the initial root width x^* (see Figs. 4 and 7). For small thickening factor, γ, we can fit this temperature evolution by a simple exponential equation: $T^* = T^*_\infty + (T^*_0 - T^*_\infty)\exp(-At^*)$, where T^*_0 and T^*_∞ are the initial and equilibrium temperatures at $0.9z^*_{eq}$. This exponential curve recalls the long term thermal evolution in a conductive layer [28]. The destabilization duration directly derives

Table 5
Simulation table for a fluid with a viscosity following an Arrhenius law

n^0	E^*	V^*	Ra_{BL}	Φ^*_{eq}	ν^*_{BL}	z^*_{eq}	T^*_i	γ	x^*	Heating
20[a]	18.7	8.04	2.27×10^9	8.4	$10^{-9.88}$	0.09	0.742	1.5	w.b.l.	internal
21[a]	18.7	8.04	2.27×10^9	8.4	$10^{-9.88}$	0.09	0.742	2.5	w.b.l., 3.53, 1.76, **0.80**, **0.40**	internal
22[a]	18.7	8.04	2.27×10^9	8.4	$10^{-9.88}$	0.09	0.742	3	w.b.l., 1.76	internal
23[b]	18.7	8.04	1.47×10^8	4.0	$10^{-6.87}$	0.18	0.727	2.5	**0.40**, **0.20**, **0.12**	basal
24[b]	18.7	8.04	4.63×10^9	5.0	$10^{-8.49}$	0.15	0.729	2.5	**0.80**, **0.40**, **0.20**	basal
25[c]	17.5	3.54	3.37×10^8	7.63	$10^{-10.30}$	0.13	0.916	2.5	w.b.l., 1.50, 0.50, **0.30**, **0.20**	internal
26[d]	9.8	3.95	1.71×10^8	6.51	$10^{-13.20}$	0.13	0.794	2	w.b.l., **0.60**	internal
27[e]	9.8	6.69	6.67×10^7	6.00	$10^{-12.62}$	0.14	0.800	2	w.b.l., 1.50, **0.30**	internal

[a] 51×201 grid mesh, aspect ratio 4.
[b] 51×151 grid mesh, aspect ratio 3.
[c] EBA.
[d] Non-Newtonian.
[e] Non-Newtonian and EBA.
See also caption of Table 4.

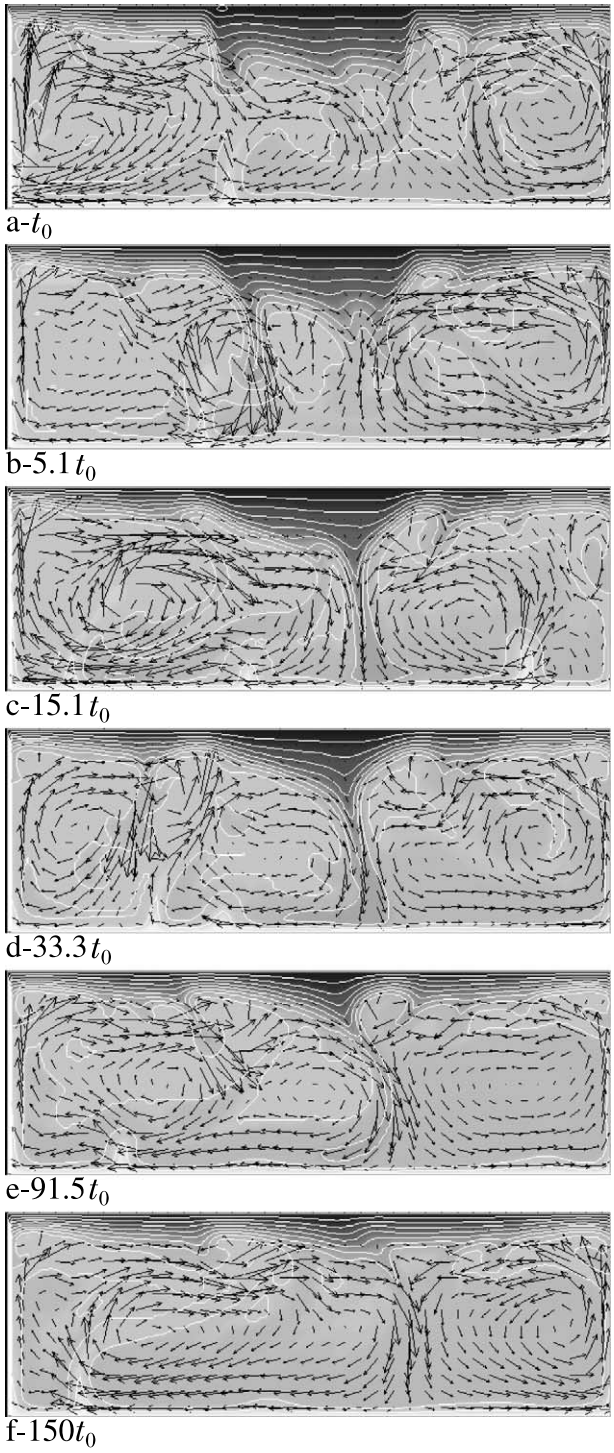

Fig. 2. Evolution of temperature field, after thickening by a factor 2.5, shown at different time steps ($t^*_0 = 10^{-4}$, scaled to $t_0 \approx 1.6$ Myr). The width and thickness of display boxes are 3 and 1, respectively. This simulation corresponds to case 8 in Table 4, with $x^* = 1$ and $b = 13$.

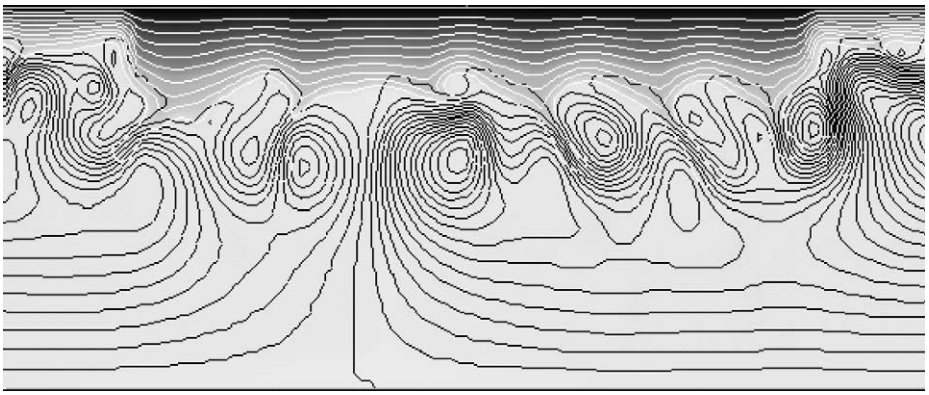

Fig. 3. Zoom of the isotherms (white lines) and the streamlines (black lines) during the removal of the thickened lithosphere. The width and thickness of display box are 2.4 and 1, respectively. Both sublithospheric convection and edge driven small-scale convection erode the lithospheric root (case 21 in Table 5, with $x^* = 1.76$).

from the fit:

$$t^*_{2-D} = \frac{1}{A} \tag{12}$$

For a large thickening factor, the exponential curve is delayed by t^*_1. This initial delay is due to the characteristic conductive time through the thickened root. Therefore, we fit only a part of the curve using: $T^*_{(t^*>-t^*_1)} = T^*_\infty + (T^*_1 - T^*_\infty)\exp(-A(t^* - t^*_1))$, where T^*_1 is the temperature reached at t^*_1 and A is calculated by the fit. The removal duration is then the sum of two terms:

$$t^*_{2-D} = t^*_1 + \frac{1}{A} \tag{13}$$

3. Thinning by sublithospheric localized convection

In this section, we describe a simplified one-dimensional (1-D) conductive model that simulates the thinning of the root by sublithospheric localized convection. We will compare this model to results of 2-D simulations in which, to avoid edge effects, the lithosphere is initially thickened through the whole box.

3.1. 1-D conductive model

In cases where the lithospheric root thinning is due to localized convection from beneath, we can model the thermal evolution of the m.b.l. by solving the 1-D heat conduction equation with an appropriate bottom boundary condition. This boundary condition should parameterize the heat supply by convection below the m.b.l. The plate model assumes that convection maintains a constant temperature at a given equilibrium depth [34]. Obviously this model does not apply to our simulations. Another bottom boundary condition

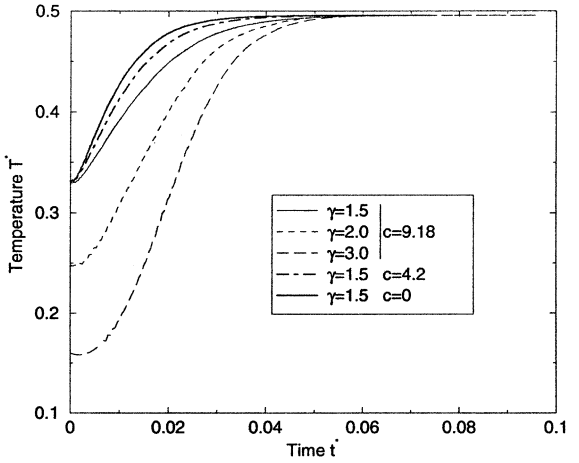

Fig. 4. Temperature evolution with time, at $z^* = 0.9z^*_{eq}$, predicted by the 1-D conductive model. Curves are displayed for different thickening factors γ and different depth dependence of the viscosity c.

is to apply a constant heat flow Φ at the base of the m.b.l. (CHABLIS model, [35]). However, the heat supplied by localized convection is likely to be a function of the viscosity below the root, ν_{BL} (see Eqs. 3 and 7), that varies with the root thickness. In a modified CHABLIS model, the heat flow Φ varies with $\nu_{BL}^{-1/3}$. Dumoulin et al. [36] compared the predictions of these three conductive models to the cooling of an oceanic lithosphere above a convective mantle. They found that the modified CHABLIS model yields a better fit to the convective simulations. Here we will compare the root thinning time scales predicted by the modified CHABLIS model to that obtained in convection simulations.

We solve the 1-D conduction equation in a dimensionless form:

$$\frac{\partial^2 T^*}{\partial z^{*2}} - \frac{\partial T^*}{\partial t^*} + q^* = 0 \tag{14}$$

The initial condition ($t^* = 0$) is given by the lithospheric equilibrium state thickened by a factor γ, (i.e. $T^* = z^* T^*_i / (\gamma z^*_{eq})$, without internal heating). The bottom boundary condition consists in applying a heat flow, Φ^*, along the base of the m.b.l., i.e. at the depth of the isotherm T^*_q:

$$T^*_q = T^*_i - \Delta T^*_{eff} = T^*_i - 2.24\delta T^*_\nu \tag{15}$$

When the viscosity depends strongly on temperature, ΔT^*_{eff} equals $2.2\delta T^*_\nu$ [25,26,30]. The temperature T^*_q corresponds approximately to the base of the rigid lid, defined as the limit where heat is transferred half by conduction and half by convection. The depth of this isotherm, z^*_{is}, decreases with time. The applied heat flow variation with depth depends on the viscosity at the base of the t.b.l.:

$$\Phi^*(z^*_{is}) = \Phi^*_{eq}\left(\frac{\nu(z^*_{is})}{\nu(z^*_q)}\right)^{1/3}$$

$$= \Phi^*_{eq}\exp\left(\left(1-\frac{z^*_{is}}{z^*_q}\right)\frac{c z^*_{eq}}{3}\right) \tag{16}$$

where z^*_q is the depth of the isotherm T^*_q at equilibrium. The equivalent value of c for an Arrhenius rheology is equal to $\frac{nV^*}{T^*_i + T^*_0}$.

Fig. 4 shows the temperature evolution versus time, computed at a depth close to the equilibrium lithospheric depth ($z^* = 0.9 z^*_{eq}$), for different values of thickening factor, γ, and depth dependence of the viscosity, c. After some time, the lithosphere reaches an equilibrium state ($T^* = z^* T^*_i / z^*_{eq} = z^* \Phi^*_{eq}$, without internal heating). The characteristic time scale, t^*_{1-D}, is calculated in the same way as for convective simulations (see Section 2.4, Eqs. 12 and 13).

We compare the time necessary to reach equilibrium, t^*_{1-D}, with a gross estimate derived from a scaling analysis, t^*_c. The total amount of heat transferred by localized convection at the base ($x^* \Phi^* t^*_c$) minus that lost at the surface ($x^* \Phi^*_s t^*_c$) during t^*_c is equal to the amount of heating within the root area

$$x^*\left(\int_0^{\gamma z^*_q}\left(1-\frac{z^*}{\gamma z^*_q}\right)T^*_q dz^* - \int_0^{z^*_q}\left(1-\frac{z^*}{z^*_q}\right)T^*_q dz^*\right),$$

where Φ^*_s is the surface heat flow. Heating near the surface is delayed compared to the lithospher-

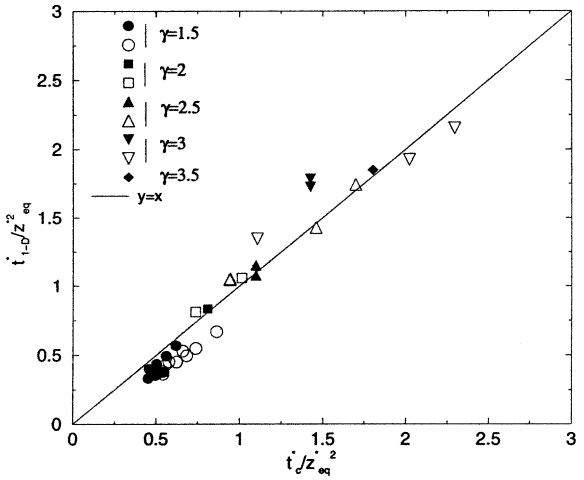

Fig. 5. Destabilization duration computed using the 1-D conductive model, t^*_{1-D}, as a function of that derived from a simple scaling analysis, t^*_c, for various depth dependences of the viscosity c (varying between 0 and 9.3), temperature scales δT^*_ν, and thickening factor γ. Filled symbols: $11.1 < \delta T^{*-1}_\nu < 18$. Open symbols: $21.4 < \delta T^{*-1}_\nu < 24.7$.

ic root heating, leading to the approximation: $\Phi^*_s \approx \Phi^*_{eq}/\gamma$. The heat flow supplied at the base of the unstable root, Φ^*, increases with time as the viscosity at the lithospheric base decreases. It is bracketed by the heat flow at the base of the thickened root, $\Phi^*_{eq}\exp(-cz^*_{eq}(\gamma-1)/3)$, and the heat flow beneath the equilibrated lithosphere, Φ^*_{eq}. We use $\Phi^* \approx \Phi^*_{eq}\exp(-cz^*_{eq}(\gamma-1)/4)$. Finally, we get:

$$t^*_c \approx \frac{(\gamma-1)\left(1-\frac{\Delta T^*_{eff}}{T^*_i}\right)^2 z^{*2}_{eq}}{2\left[exp\left(\frac{cz^*_{eq}(1-\gamma)}{4}\right)-\frac{1}{\gamma}\right]} \quad (17)$$

where $(1-\Delta T^*_{eff}/T^*_i)$ is a corrective term introduced because the bottom boundary condition is not applied exactly along $T^* = T^*_i$ but at a shallower depth corresponding to $T^* = T^*_q$. t^*_c is then proportional to the square of the conductive lid thickness at equilibrium, $(1-\Delta T^*_{eff}/T^*_i)z^*_{eq}$. The effect of internal heating is neglected in this relationship. Note that when the heat supplied by localized convection at the base of the thickened root ($\Phi^*_{eq}\exp(-cz^*_{eq}(\gamma-1)/3)$) is equal or lower than that transferred by conduction across the root (Φ^*_{eq}/γ), t^*_c becomes infinite or even negative. This means that the root is stable or could grow further. This can occur when the mantle viscosity strongly increases with depth [20].

On Fig. 5, t^*_{1-D} is plotted as a function of t^*_c. t^*_{1-D} approximately follows the predicted relationship: $t^*_{1-D} \approx t^*_c$. Differences, however, come from the oversimplified way of estimating t^*_c.

3.2. Comparison between 2-D convective simulations and 1-D conductive models

We examine here only the simulations where the lithosphere has been thickened over the whole box length. On Fig. 6, we compare t^*_{2-D} to the value predicted by the 1-D conductive model, t^*_{1-D}. In cases with a low thickening factor and a moderately temperature dependent viscosity or in all cases with a strongly temperature dependent viscosity (Arrhenius rheology or $b = 18$), t^*_{2-D} falls within $\pm 20\%$ of the predicted values. However, when the viscosity contrast across the lithosphere is relatively small ($b = 13$) and when the thickening factor is large, the destabilization time is about 40% smaller than predicted (filled circles on Fig. 6). As discussed above, in these cases, we cannot neglect whole-scale lithospheric deformation. This yields a departure from the 1-D conductive model, which assumes the existence of a rigid layer with a laterally uniform temperature structure overlying an unstable lithospheric sublayer with a small temperature drop ΔT^*_{eff}.

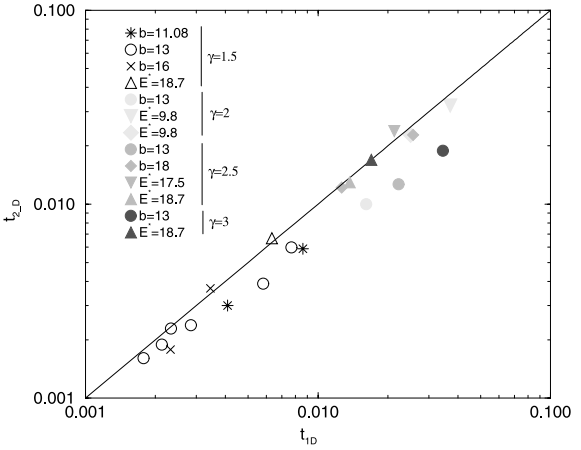

Fig. 6. Comparison of the destabilization duration t^*_{2-D} calculated from convective simulations with that predicted using the 1-D conductive code, t^*_{1-D}. Each point corresponds to a simulation (cases 1–3, 5–9, 11–14, 17–22, 25–27 listed in Tables 4 and 5) where the root has been thickened over the whole box length.

Fig. 6 shows that the order of the destabilization duration is well predicted by the 1-D conductive model even in the EBA and in the non-Newtonian rheology cases (cases 25, 26, and 27 listed in Table 5). This agreement indicates that root thinning by sublithospheric convection can simply be parameterized by the effect of a heat flow Φ^* applied at the base of the m.b.l. and that Φ^* depends on the asthenospheric viscosity (Eq. 11).

4. Root shortening by convection on the root edges

4.1. Influence of the initial root width and of the thickening factor

For narrow lithospheric roots the flow along its

sides becomes the dominant mechanism of convective removal. To study this mechanism, we computed the characteristic destabilization times t^*_{2-D} for different widths x^* and different thickening factors (cases 4, 8, 15, 16, 21, 23–27 listed in Tables 4 and 5). For example, the temperature evolution with time after an instantaneous thickening is displayed on Fig. 7 for five initial root widths, all other parameters being the same. The temperature at $z^* = 0.9z^*_{eq}$, once the thermal equilibrium is reached, presents variations of $\pm 10\%$ that depend on the root location and width. These strong temperature heterogeneities are due to the isotherm topography near the base of the lithosphere. They introduce uncertainties in the evaluation of t^*_{2-D} (see Fig. 8). Despite these uncertainties, Fig. 7 shows clearly that the root longevity increases with x^* for small widths, and that for larger widths it reaches an asymptotic value equal to that obtained when the lithosphere is thickened through the whole box. This illustrates the transition between the two removal mechanisms, convection mainly driven by density contrast across the root edges to sublithospheric convection driven by density contrasts at the lithospheric base.

For small widths we find that t^*_{2-D} is roughly proportional to x^*, implying an almost constant velocity for the root width reduction. Note that here t^*_{2-D} is computed using the temperature

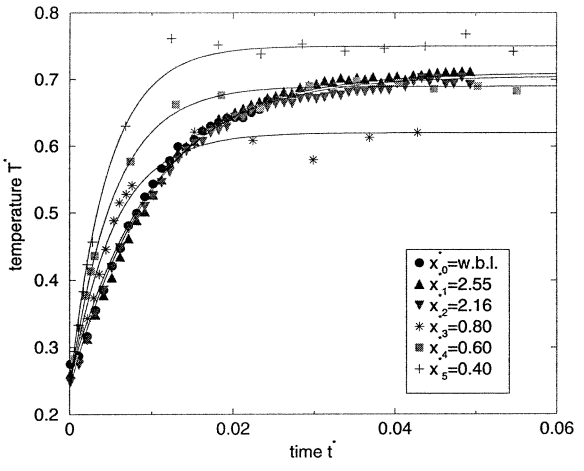

Fig. 7. Temperature evolution with time, computed at $z^* = 0.9z^*_{eq}$, for five different root widths (case 8 in Table 4).

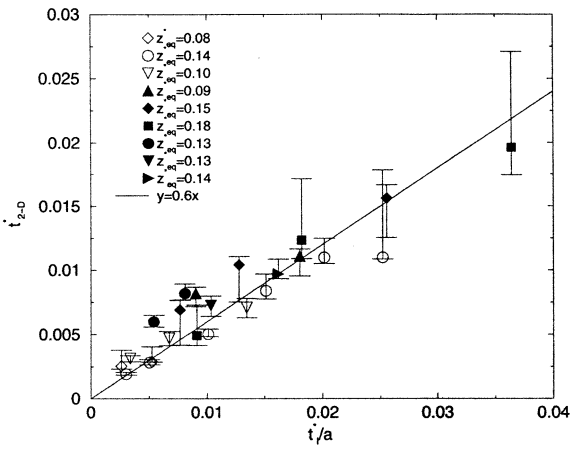

Fig. 8. Convective duration, t^*_{2-D}, versus the duration deriving from a scaling analysis, t^*_1 (cases 4, 8, 15, 16, 21, 23–27 listed in Tables 4 and 5). A linear regression of the form $y = ax$ yields $a = 0.6$.

evolution at a depth close to the base of lithosphere at equilibrium (at $z^* = 0.9z^*_{eq}$). The return towards equilibrium at depth shallower than about $0.5z^*_{eq}$ is controlled by conduction within the lid. Therefore, the destabilization duration, when computed using the temperature evolution at a shallow depth, is larger than that computed at $z^* \approx z^*_{eq}$. This delay does not tend to zero when the width tends to zero. This is the reason why we choose to measure t^*_{2-D} near $z^* = z^*_{eq}$.

4.2. General relationship for erosion on the root sides

We compare the destabilization duration, t^*_{2-D}, obtained by 2-D convective simulations with that deriving from a simple scaling analysis, t^*_1. We consider here that the total amount of heat transferred during t^*_1 through the root edges, $2t^*_1(\gamma-1)z^*_{eq}\Phi^*_1$, equals the amount of heating within the root area, where Φ^*_1 is the lateral heat transfer. We neglect heating and cooling of the root by its base and surface, respectively. Furthermore, we write that Φ^*_1 is proportional to the basal heat flow transferred by localized convection ($\Phi^*_1 = (1/a)\Phi^*$). We obtain:

$$t^*_1 = \frac{a}{4}\frac{T^*_i}{\Phi^*_{eq}}x^*\left(1-\frac{\Delta T^*_{eff}}{T^*_i}\right)^2\exp\left(\frac{cz_{eq}(\gamma-1)}{4}\right) \qquad (18)$$

All destabilization durations falling in the regime where the main destabilization mechanism is due to flow on the root sides have been plotted on Fig. 8. They result from simulations with different initial root widths, thickening factors, equilibrium thicknesses and rheologies (Newtonian and non-Newtonian). Despite strong uncertainties on the determination of t^*_{2-D}, it correlates well with the predicted relationship, yielding $a \approx 0.6$. It indicates that the destabilization on the root sides is 1.5 more efficient than at the base.

4.3. Aspect ratio defining the transition between the two removal mechanisms

On Fig. 9, the destabilization duration computed from convective simulations divided by that predicted using the 1-D conductive model, t^*_{2-D}/t^*_{1-D}, is displayed as a function of the aspect ratio of the thickened root, $r = x^*/z^*_{eq}(\gamma-1)$. For aspect ratios $r < r_0$, the main removal mechanism is due to small-scale convection on the root edges ($(t^*_{2-D}/t^*_{1-D}) < 1$), whereas for $r > r_0$, the main removal mechanism is due to small-scale sublithospheric convection ($(t^*_{2-D}/t^*_{1-D}) \simeq 1$). The limit aspect ratio r_0 varies with c and γ as:

$$r_0 \simeq 3.33\left[1-\frac{\exp(cz^*_{eq}(\gamma-1)/4)}{\gamma}\right]^{-1} \quad (19)$$

5. Scaling to the Earth's mantle

5.1. Scaling problem

Convective removal durations that have been inferred by modeling studies range from a few Myr to some Gyr (e.g. [7,13–15]). To understand the discrepancies between various study results, we, in a first step, note that the dimensional heat flow Φ_{eq} transferred by localized convection writes as (see Eq. 11):

$$\Phi_{eq} \approx kT_i/z_{eq} \approx 0.5k\left(\frac{\alpha\rho g}{\kappa\nu_{BL}}\right)^{1/3}\delta T_\nu^{4/3} \quad (20)$$

If different numerical experiments are all scaled

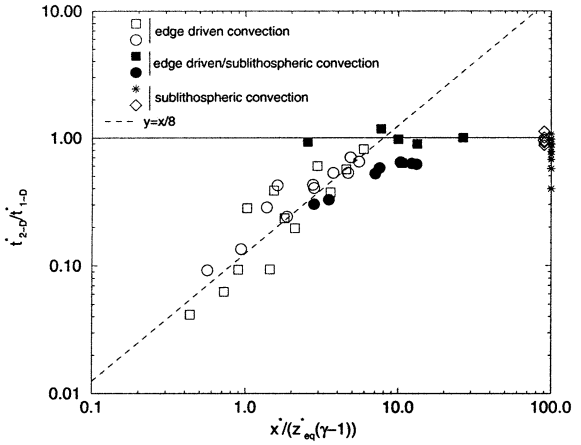

Fig. 9. Convective duration divided by duration predicted by the 1-D conductive model (t^*_{2-D}/t^*_{1-D}), versus the aspect ratio of the thickened zone, $x^*/z^*_{eq}(\gamma-1)$. Filled squares, open squares, and open diamonds: Arrhenius viscosity law. Filled circles, open circles, and stars: viscosity depending exponentially on temperature and depth.

using a given box height (H), resulting characteristic heat flows (Φ_{eq}), equilibrium lithospheric thicknesses, and removal durations will strongly depend on the values of ν_{BL} and δT_ν. For example, for large values of ν_{BL} and/or low values of δT_ν, a 300 km thick lithosphere can be inferred to be indefinitely stable [15,37]. If this is the case, a lithosphere initially thinner than 300 km will cool and grow until the decreasing conductive heat transfer through the rigid part of the lithosphere reaches heat transferred by localized convection. On the contrary, for lower values of ν_{BL} and/or larger values of δT_ν, a 300 km thick lithosphere could be inferred to be unstable and the time necessary to reach back its thinner equilibrium state would strongly depend on Φ_{eq} (or z_{eq}).

In order to obtain dimensional removal duration, we prefer to use an approximate value of the heat flow supplied by localized convection in the Earth's mantle, $\Phi_{eq} = 40$ mW/m^2 (or $z_{eq} \approx 100$ km, see Section 5.2). Using the activation energy and volume for wet (dry, respectively) olivine given by [38] and Eq. 8, we obtain $\delta T_\nu^{wet} = 85$ K ($\delta T_\nu^{dry} = 70$ K, respectively) yielding $\Delta T_{eff}^{wet} = 190$ K ($\Delta T_{eff}^{dry} = 160$ K, respectively). Eq. 20 then implies an asthenospheric viscosity of 3×10^{18} Pa s for wet olivine and of 1.4×10^{18} Pa s for dry olivine

(see Table 2). This viscosity (at $T_m \simeq 1600$ K) is consistent with that measured on wet peridotite, but it is lower than that measured on dry peridotite [19]. However, the presence of such a low viscosity zone agrees with recent dynamic modeling using geoid, topography, and plate velocity [39] and with postglacial rebound data [40–42].

5.2. Heat transferred by localized convection

Large-scale convection currents within the mantle related to accretion and subduction could be considered, in the uppermost mantle away from plate boundaries, as a horizontal translation with a negligible shearing component. Within such a flow the lithosphere/asthenosphere system should cool purely by conduction. This cooling mode implies that oceanic and continental basins should continuously subside since the last extension event and that surface heat flow in the oceanic basin should continuously decrease with age. However, subsidence in oceanic and young continental basins, heat flow, and geoid indicate that the cooling of the lithosphere slows down with respect to the purely conductive half-space model predictions, and eventually stops (referred to as 'flattening' in the literature) (e.g. [34,35,43–46]). Most lithospheric cooling models employed to fit these data thus yield after 60–300 Myr a steady lithospheric thermal state such that heat transferred at the base of the conductive lithosphere is equal to heat lost at the surface plus the radioactive heat produced within the lithosphere. This heat transfer is evaluated to about 35–50 mW/m^2. The corresponding 'plate' lithospheric thickness, defined as the depth at which the conductive geotherm crosses the adiabat, is then 90–130 km (e.g. [35,43–45]).

Heat provided at the base of the lithosphere can originate from shear heating or from heat advection by basal drag, hot upwellings, and localized convection. Heat transfer due to shear heating or basal drag depends on the absolute plate velocity. However, the 'flattening' does not differ from slow to rapid plates. Furthermore, ponding of hot material below the lithosphere does not alter much its thermal state, unless enhanced localized convection develops due to the viscosity decrease below the lithosphere [47]. We therefore consider that the heat transfer through lithospheric plates at thermal equilibrium is due to localized convection [20,25,28].

5.3. Root destabilization time scale

The dimensional removal duration derived from Eqs. 17 and 18, without taking into account internal heating, writes as:

$$t_{2-D} \approx \frac{z_{eq}^2(\gamma-1)\left(1-\frac{\Delta T_{eff}}{T_i}\right)^2}{2\kappa\left[\exp\left(\frac{V\rho g z_{eq}(1-\gamma)}{4R(T_i+T_0)}\right)-\frac{1}{\gamma}\right]} \quad (21)$$

when the main removal mechanism is thinning by sublithospheric small-scale convection, and as:

$$t_{2-D} \approx \frac{0.15 z_{eq} x}{\kappa \exp\left(\frac{V\rho g z_{eq}(1-\gamma)}{4R(T_i+T_0)}\right)}\left(1-\frac{\Delta T_{eff}}{T_i}\right)^2 \quad (22)$$

when the main removal mechanism is shortening by edge driven small-scale convection. Therefore, the dimensional destabilization time depends only on local parameters defined in the lithosphere/asthenosphere system, and does not depend on the height of the box, H, or on the total temperature drop across the box, ΔT.

The width of the thickened zone that limits the two domains is given by:

$$x_0 = \frac{3.33 z_{eq}(\gamma-1)}{\left(1-\frac{1}{\gamma}\exp\left(\frac{V\rho g z_{eq}(\gamma-1)}{4R(T_0+T_i)}\right)\right)} \quad (23)$$

Using the parameters listed in Table 2, an initially 150 km thick lithosphere reaches back its equilibrium in 300 Myr if it thins by sublithospheric convection (for an initial root width larger than 840 km), and in 40 Myr for an initial root width of 100 km if it shortens by edge driven convection. The removal duration for a 300 km thick lithosphere wider than 1750 km by sublithospheric convection is inferred to be 1.1 Gyr.

As the activation energies measured for olivine in the dislocation creep regime times $2/n+1$ are

usually less than those measured in the diffusion creep regime, the effective temperature drop (Eq. 8) for a non-Newtonian rheology (~290 K) is inferred to be greater than that for a Newtonian rheology (~160–190 K). Using Eqs. 21 and 22 the estimated destabilization durations are then only slightly smaller (by about 20%) for a non-Newtonian rheology than for a Newtonian rheology. Inspection of Eqs. 21 and 22 shows that, for small effective temperature drops, the estimated removal durations will mostly and very strongly depend on the chosen value for z_{eq}.

6. Discussion

Our results are in good agreement with other studies, which show that only a thin layer, located at the base of the lithosphere and characterized by a small temperature drop (ΔT_{eff} in this paper), can be quickly removed and that the characteristic removal duration of a whole lithospheric root is related to the heat conduction time scale [7,9].

Marotta et al. [13,14] did not emphasize the importance of employing a realistic rheology to determine the destabilization duration. The simulation that they show and discuss in details (referred as MOD-8 in [13]) is conducted with a weak temperature dependence of the viscosity, yielding ΔT_{eff} equal to 1400 K. The unstable lithospheric sublayer then becomes nearly the whole lithosphere, which is easily and quickly removed. They therefore found a destabilization duration of less than 10 Myr. The minimum value of ΔT_{eff} that they employed in their simulations is 500 K. In these cases, they observe an instability that only affects the lower third of the lithosphere.

In Houseman and Molnar [48] and Molnar et al. [49], scaling laws are derived for the growing time scale of a Rayleigh–Taylor instability, ignoring thermal diffusion and the effect of temperature advection on the viscosity structure of the developing drip. Both effects should delay or could even annihilate any instability growth. Indeed, neglecting thermal diffusion, any temperature perturbation is unstable, whereas when thermal diffusion is taken into account, a perturbation grows when the Rayleigh number is larger than the critical Rayleigh number. Conrad and Molnar [50] found that, for sufficiently high Ra and for a given perturbation wavelength, the growth rate of the perturbation becomes independent from thermal diffusion (fig. 9, eq. 25 in [50]). However, the wavelength corresponding to the maximum growth rate strongly decreases with the viscosity contrast. For these smaller wavelengths, heat diffusion may not be neglected.

Marotta et al. [13,14], Houseman and Molnar [48], Molnar et al. [49] and Conrad and Molnar [50] do not describe the long term lithospheric evolution, but focus on the development of the first dripping instability. They find that the first drip at the base of the lithosphere develops in about 10 Myr. However, the formation of a first drip does not preclude for the lithospheric root evolution. For example a lithosphere could continue to cool after the first drip development [36,51]. When a drip only affects a small ΔT_{eff}, the effect of many successive drips is necessary to erode a thickened lithosphere, and it should overcome the growing of the lithosphere by thermal diffusion. Therefore, we consider that their studies do not apply to the stability/removal problem of a thermally thickened lithospheric root, unless the upper most mantle rheology implies much larger values of ΔT_{eff} than calculated here.

7. Conclusion

This article mainly proposes two empirical parameterizations of the convective removal duration of a thickened continental lithosphere. Because of uncertainties on the evaluation of this duration linked to temperature fluctuations in a chaotic environment, these relationships remain approximate. However, they yield the order of magnitude of the involved time scales and help to assess the main convective removal mechanisms.

The lithospheric root shrinks progressively thanks to the repeated development of instabilities due to lateral density contrast at the edge of the root and due to the density gradient at the base of the root. A limit root aspect ratio, r_0, separates two domains: (1) the root mainly thins by sub-

lithospheric convection ($r > r_0$). Its evolution can be described by a 1-D conductive model (CHABLIS modified model, [19]). This shows that thinning is triggered by heat transfer due to small-scale convection at the base of the lithosphere. (2) The root mainly shortens by edge driven convection ($r < r_0$). The removal duration is then proportional to the width of the thickened zone and one can define a constant erosion velocity.

For both removal mechanisms, root destabilization is due to small-scale convective processes and depends only on local parameters characterizing the lithosphere/asthenosphere system. For a viscous temperature scale of 85 K, and depending on the assumed value for the asthenospheric viscosity, ν_{BL}, a 250 km thick lithospheric root could be inferred to thicken ($\nu_{BL} > 4.7\times10^{19}$ Pa s) or to be stable ($\nu_{BL} = 4.7\times10^{19}$ Pa s) or to be removed in a few tens to hundreds of Myr ($\nu_{BL} < 4.7\times10^{19}$ Pa s). The relationships 8 and 20 allow to predict this behavior for any activation energies and any asthenospheric viscosities. Following for example Davaille and Jaupart [25] and Parsons and McKenzie [28], we consider that the asthenospheric viscosity is such that small-scale convection limits the thickness of a cooling (undepleted or only slightly depleted) lithosphere to a maximum of about 100 km.

Small-scale convective processes should then progressively and completely thin a 250 km thick lithosphere (thickened for example by orogenic processes) in about 55–750 Myr depending on the root width. Furthermore, the erosion velocity on each root side is about 0.8 mm/yr. Convective interactions in a purely ductile upper mantle cannot therefore be invoked to explain the sudden mantle lithosphere delamination event that may have occurred in Tibet. Note that if the mantle lithosphere has been thickened by underthrusting beneath a few isolated successive suture zones, yielding to a few isolated 100 km wide roots, the removal duration is estimated to about 40–60 Myr. On the other hand, the above mentioned convective thinning and shortening rates are at odds with the cratonic roots long term stability. Indeed, a close geographic adjustment is observed between the borders of the cratonic crust and of the cratonic root around the Kaapvaal craton [52]. Furthermore, some Archean roots did not experience any significant thinning since 2–3 Gyr [53,54]. Therefore, if we accept that the thermal equilibrium thickness of the lithosphere is lower than 150 km, these cratonic roots must be stabilized against convective removal by the buoyancy and viscosity increase due to depletion of the cratonic lithosphere [15,20,55,56].

In this study, we focused on the parameterization of the convective removal of a lithospheric root and neglected tectonic deformation. This was achieved by using realistic viscous rheologies for a peridotite upper mantle that generates a rigid lid at the surface. To obtain plate-like tectonic deformation in numerical modeling, it seems important to combine a brittle rheology with a temperature dependent viscous behavior [57–59]. However, this, to our knowledge, has yet been obtained only for a viscosity that depends too moderately on temperature. As argued by Lenardic and Moresi [37], future studies aimed at studying lithospheric root destabilization by both whole-scale lithospheric deformation and small-scale convection should include a strongly temperature dependent viscosity combined with the weakening effect of the crust and of the brittle rheology. This approach has been undertaken by Schott and Schmeling [7]. They find that the lithospheric root can delaminate very quickly when they impose an extremely weak brittle rheology (with pore pressure equal to 0.97 times the lithostatic pressure) in a deep domain on one side of the lithospheric root to initiate delamination.

Acknowledgements

We thank Luce Fleitout for helpful discussions, and Gabrielle Marquart and Bertram Schott for their helpful comments on the manuscript. This work was supported by the CNRS-INSU-IT program.*[AC]*

References

[1] J. Platt, P. England, Convective removal of lithosphere beneath mountain belts: thermal and mechanical consequences, Am. J. Sci. 293 (1993) 307–336.

[2] J. Dewey, Extensional collapse of orogens, Tectonics 7 (1988) 1123–1139.
[3] P. England, G. Houseman, Extension during continental convergence, with application to the Tibetan Plateau, J. Geophys. Res. 94 (1989) 17561–17579.
[4] P. England, Convective removal of thermal boundary layer of thickened continental lithosphere: a brief summary of causes and consequences with special reference to the Cenozoic tectonics of the Tibetan Plateau and surrounding regions, Tectonophysics 223 (1993) 67–73.
[5] V. Levin, J. Park, M.T. Brandon, W. Menke, Thinning of the upper mantle during late Paleozoic Appalachian orogenesis, Geology 28 (2000) 239–242.
[6] P. Bird, J. Baumgardner, Steady propagation of delamination events, J. Geophys. Res. 86 (1981) 4891–4903.
[7] B. Schott, H. Schmeling, Delamination and detachment of a lithospheric root, Tectonophysics 296 (1998) 225–247.
[8] G. Houseman, D. McKenzie, P. Molnar, Convective instability of a thickened boundary layer and its relevance for the thermal evolution of continental convergence belts, J. Geophys. Res. 86 (1981) 6115–6132.
[9] W. Buck, M. Toksöz, Thermal effects of continental collisions: thickening a variable viscosity lithosphere, Tectonophysics 100 (1983) 53–69.
[10] L. Fleitout, D. Yuen, Steady state, secondary convection beneath lithospheric plates with temperature- and pressure-dependent viscosity, J. Geophys. Res. 89 (1984) 9227–9244.
[11] C. Jaupart, B. Parsons, Convective instabilities in a variable viscosity fluid cooled from above, Phys. Earth Planet. Inter. 39 (1985) 14–32.
[12] L.-N. Moresi, V.S. Solomatov, Numerical investigation of 2D convection with extremely large viscosity variations, Phys. Fluids 7 (1995) 2154–2162.
[13] A. Marotta, M. Fernàndez, R. Sabadini, Mantle unrooting in collisional settings, Tectonophysics 296 (1998) 31–46.
[14] A. Marotta, M. Fernàndez, R. Sabadini, The onset of extension during lithospheric shortening: a two-dimensional thermomechanical model for lithospheric unrooting, Geophys. J. Int. 139 (1999) 98–114.
[15] S. Shapiro, B. Hager, T. Jordan, Stability and dynamics of the continental tectosphere, Lithos 48 (1999) 115–133.
[16] B. Meyer, P. Tapponnier, L. Bourjot, F. Métivier, Y. Gaudemer, G. Peltzer, G. Shunmin, C. Zhitai, Crustal thickening in Gansu-Qinghai, lithospheric mantle subduction, and oblique, strike-slip controlled growth of the Tibet plateau, Geophys. J. Int. 135 (1998) 1–47.
[17] U. Christensen, Convection with pressure- and temperature-dependent non-Newtonian rheology, Geophys. J. R. Astron. Soc. 77 (1984) 343–384.
[18] F.M. Richter, H.C. Nataf, S.F. Daly, Heat transfer and horizontally averaged temperature of convection with large viscosity variations, J. Fluid Mech. 129 (1983) 173–192.
[19] C. Dumoulin, M.-P. Doin, L. Fleitout, Heat transport in stagnant lid with temperature and pressure dependent Newtonian or non-Newtonian rheology, J. Geophys. Res. 104 (1999) 12759–12778.
[20] M.-P. Doin, L. Fleitout, U. Christensen, Mantle convection and stability of depleted and undepleted continental lithosphere, J. Geophys. Res. 102 (1997) 2771–2787.
[21] K.C. Stengel, D.S. Oliver, J.R. Booker, Onset of convection in a variable viscosity fluid, J. Fluid Mech. 120 (1982) 411–431.
[22] A.C. Fowler, Fast thermoviscous convection, Stud. Appl. Math. 72 (1985) 189–219.
[23] S. Morris, D. Canright, A boundary-layer analysis of Benard convection in a fluid of strongly temperature-dependent viscosity, Phys. Earth Planet. Inter. 36 (1984) 355–373.
[24] H.C. Nataf, Eléments d'anatomie et de physiologie du manteau terrestre-tomographie sismique et convection expérimentale, thèse d'état, Université Paris VI, 1986.
[25] A. Davaille, C. Jaupart, Onset of thermal convection in fluids with temperature-dependent viscosity: application to the oceanic mantle, J. Geophys. Res. 99 (1994) 19853–19866.
[26] V.S. Solomatov, L.N. Moresi, Scaling of time-dependent stagnant lid convection: application to small-scale convection on Earth and other terrestrial planets, J. Geophys. Res. 105 (2000) 21795–21817.
[27] L. Howard, Convection at high Rayleigh number, In: H. Gortler (Ed.), Proceedings of the 11th International Congress on Applied Mechanics, Springer-Verlag, New York, 1964, pp. 1109–1115.
[28] B. Parsons, D. McKenzie, Mantle convection and the thermal structure of the plates, J. Geophys. Res. 83 (1978) 4485–4496.
[29] V.S. Solomatov, Scaling of temperature- and stress-dependent viscosity convection, Phys. Fluids 7 (1995) 266–274.
[30] O. Grasset, E.M. Parmentier, Thermal convection in a volumetrically heated, infinite Prandtl number fluid with strongly temperature-dependent viscosity: Implications for planetary thermal evolution, J. Geophys. Res. 103 (1998) 18171–18181.
[31] C. Dumoulin, Convection mantellique et structure de la lithosphère, thèse d'état, Université Paris XI, 2000.
[32] D.A. Yuen, L. Fleitout, Stability of the oceanic lithosphere with variable viscosity: an initial-value approach, Phys. Earth Planet. Inter. 343 (1984) 173–185.
[33] S. King, J. Ritsema, African hot spot volcanism: small-scale convection in the upper mantle beneath cratons, Science 290 (2000) 1137–1140.
[34] B. Parsons, J.G. Sclater, An analysis of the variation of ocean floor bathymetry and heat flow with age, J. Geophys. Res. 82 (1977) 803–827.
[35] M.-P. Doin, L. Fleitout, Geoid anomalies and the structure of continental and oceanic lithospheres, J. Geophys. Res. 101 (1996) 16119–16135.
[36] C. Dumoulin, M.-P. Doin, L. Fleitout, Numerical simulations of the cooling of an oceanic lithosphere above a convective mantle, Phys. Earth Planet. Inter. 125 (2001) 45–64.

[37] A. Lenardic, L.-N. Moresi, Some thoughts on the stability of cratonic lithosphere: Effects of buoyancy and viscosity, J. Geophys. Res. 104 (1999) 12747–12758.
[38] S. Karato, P. Wu, Rheology of the upper mantle: a synthesis, Science 260 (1993) 771–778.
[39] O. Cadek, L. Fleitout, A global geoid model with imposed plate velocities and partial layering, J. Geophys. Res. 104 (1999) 29055–29075.
[40] W. Fjeldskaar, Viscosity and thickness of the asthenosphere detected from the Fennoscandian uplift, Earth Planet. Sci. Lett. 126 (1994) 399–410.
[41] G. Kaufmann, D. Wolf, Deglacial land emergence and lateral upper-mantle heterogeneity in the Svalbard Archipelago, II, Extended results for high-resolution load models, Geophys. J. Int. 127 (1996) 125–140.
[42] F. Sigmundsson, Post-glacial rebound and asthenosphere viscosity in Iceland, Geophys. Res. Lett. 18 (1991) 1131–1134.
[43] C.A. Stein, S. Stein, A model for the global variation in oceanic depth and heat flow with lithospheric age, Nature 359 (1992) 123–129.
[44] C. Prijac, M. Doin, J. Gaulier, F. Guillocheau, Subsidence of the Paris Basin and its bearing on the late Variscan lithosphere evolution: a comparison between Plate and Chablis models, Tectonophysics 323 (2000) 1–38.
[45] N. White, An inverse method for determining lithospheric strain rate variation on geological timescales, Earth Planet. Sci. Lett. 122 (1994) 351–371.
[46] M.P. Doin, L. Fleitout, Flattening of the oceanic topography and geoid: thermal versus dynamic origin, Geophys. J. Int. 143 (2000) 582–594.
[47] W.B. Moore, G. Schubert, P. Tackley, Three-dimensional simulations of plume-lithosphere interaction at the Hawaiian swell, Science 279 (1998) 1008–1011.
[48] G. Houseman, P. Molnar, Gravitational (Rayleigh–Taylor) instability of a layer with non-linear viscosity and convective thinning of continental lithosphere, Geophys. J. Int. 128 (1997) 125–150.
[49] P. Molnar, G.A. Houseman, C.P. Conrad, Rayleigh–Taylor instability and convective thinning of mechanically thickened lithosphere: effects of non-linear viscosity decreasing exponentially with depth and of horizontal shortening of the layer, Geophys. J. Int. 133 (1998) 568–584.
[50] C.P. Conrad, P. Molnar, Convective instability of a boundary layer with temperature- and strain-rate-dependent viscosity in terms of 'available buoyancy', Geophys. J. Int. 139 (1999) 51–68.
[51] G. Choblet, C. Sotin, 3d thermal convection with variable viscosity: can transient cooling be described by a quasi-static scaling law?, Phys. Earth Planet. Inter. 119 (2000) 321–336.
[52] F.R. Boyd, J.J. Gurney, Diamonds and the African lithosphere, Science 232 (1986) 472–477.
[53] S.H. Richardson, J.J. Gurney, A.J. Erlank, J.W. Harris, Origin of diamonds in old enriched mantle, Nature 310 (1984) 198–202.
[54] R.W. Carlson, A.J. Irving, Depletion and enrichment history of subcontinental lithospheric mantle: an Os, Sr, Nd and Pb isotopic study of ultramafic xenoliths from the northwestern Wyoming Craton, Earth Planet. Sci. Lett. 126 (1994) 457–472.
[55] T.H. Jordan, Composition and development of the continental tectosphere, Nature 274 (1978) 544–548.
[56] J. de Smet, A.P. van den Berg, N.J. Vlaar, Early formation and long-term stability of continents resulting from decompression melting in a convecting mantle, Tectonophysics 322 (2000) 19–33.
[57] L.-N. Moresi, V.S. Solomatov, Mantle convection with a brittle lithosphere: thoughts on the global tectonic styles of the Earth and Venus, Geophys. J. Int. 133 (1998) 669–682.
[58] P.J. Tackley, Self-consistent generation of tectonic plates in three-dimensional mantle convection, Earth Planet. Sci. Lett. 157 (1998) 9–22.
[59] R.A. Trompert, U. Hansen, Mantle convection simulations with rheologies that generate plate-like behavior, Nature 395 (1998) 686–689.